communications materials

A Nature Portfolio journal

Review article

https://doi.org/10.1038/s43246-025-00794-3

Intrinsic magnetic topological insulators of the $MnBi_2Te_4$ family

Alexandra Yu. Vyazovskaya[1], Mihovil Bosnar[2,3,7], Evgueni V. Chulkov[2,4,5] ✉ & Mikhail M. Otrokov[6] ✉

This short review appears on the occasion of the fifth anniversary of discovery of intrinsic magnetic topological insulators (MTIs) of the $MnBi_2Te_4$ family, which have attracted a great deal of attention recently. This family of materials has been discovered in attempts to increase the observation temperature of the quantum anomalous Hall effect as well as to facilitate the eventual realization of the topological magnetoelectric effect. Therefore, we first briefly introduce these effects, then describe the experimental state-of-the-art in the MTIs field just prior to $MnBi_2Te_4$ appearance, after which we discuss the basic properties of this material and its family. Finally, we overview the exciting progress made during 5 years of intense research in this field.

Introducing magnetism in a nonmagnetic topological insulator (TI) is known to give rise to fascinating and technologically promising phenomena[1,2]. One of them is the quantum anomalous Hall effect (QAHE)[3–6], which can be observed in the magnetic thin films featuring an inverted band gap due to spin-orbit coupling, i.e., two-dimensional magnetic TIs (MTIs). The bulk-edge correspondence[7] dictates that at the physical border of such materials there must be a gapless topological edge state. Remarkably, an electron moving in such a state at any given edge of the sample can propagate only in one direction and cannot backscatter. Such a chirality of the edge state makes the QAHE attractive for the dissipationless transport applications. For example, it can be used to create interconnect devices that electrically connect the components of an integrated circuit[8]. The experimental hallmark of the QAHE is a vanishing longitudinal conductivity σ_{xx} along with a transversal conductivity σ_{xy} quantized to integer multiples of the conductance quantum, Ce^2/h (for the resistivities, $\rho_{xx} = 0$ and $\rho_{yx} = h/(Ce^2)$). Here, e is the electron charge, h is the Planck's constant, and C is a dimensionless integer called the first Chern number, which is a topological invariant for these kind of systems[1,2,6].

Another fundamental phenomenon arising in MTIs is the topological magnetoelectric effect (TME)[2,9,10]. When the TI surfaces are gapped due to magnetism, it should respond to the application of an external electric (magnetic) field by generation of a (an) magnetic (electric) polarization that appears to be quantized. An intriguing TME-related phenomenon is the solid-state embodiment of the axion electrodynamics[2,11,12], arising from a peculiar analogy with a field theory, where the axion field is said to generate electrodynamics with exactly the same Lagrangian that describes the TME in TIs. A material possessing these exotic properties is called axion insulator. Other interesting implications of the unique magnetolectric properties of MTIs are the quantized Kerr and Faraday effects[2,13].

The observation of the QAHE in the Cr-doped TI $(Bi_xSb_{1-x})_2Te_3$[14,15] gave a strong impetus to a worldwide study of these systems. Nowadays, magnetically-doped TIs reproducibly show very robust high-precision QAHE at mK temperatures and they are currently being considered for metrological applications[16]. Besides, the QAHE is achieved not only in the MTIs, but also in the twisted bilayer graphene[17] and transition metal dichalcogenides heterostructures[18]. Measuring TME in a magnetic TI proved more challenging, but it was eventually achieved, too[19]. However, a random distribution of the magnetic atoms in the magnetically-doped TIs leads to strongly inhomogeneous magnetic and electronic properties of these materials[20–22], restricting the observation of these effects to very low temperatures[23]. More specifically, the atomic disorder leads to the fluctuation of both the size and energy position of the Dirac point gap across the surface of these materials, as imaged with scanning tunneling spectroscopy in ref. 20. As a consequence, this gap has not been observed in angle-resolved photoemission spectroscopy (ARPES) for Cr- or V-doped $(Bi_xSb_{1-x})_2Te_3$ with stoichiometries close to those showing QAHE[24,25].

As an alternative to the magnetically doped TIs, a new class of magnetic topological matter emerged: *intrinsic* MTI compounds, the first representative of this class being antiferromagnetic (AFM) van der Waals material $MnBi_2Te_4$[26–31]. This discovery was preceded by both theoretical and experimental studies of the magnetic topological heterostructures such as $MnBi_2Te_4/Bi_2Te_3(0001)$, $MnBi_2Se_4/Bi_2Se_3(0001)$, and others that were

[1]Tomsk State University, 634050 Tomsk, Russia. [2]Donostia International Physics Center, 20018 Donostia-San Sebastián, Spain. [3]Departamento de Polímeros y Materiales Avanzados: Física, Química y Tecnología, Facultad de Ciencias Químicas, Universidad del País Vasco UPV/EHU, 20018 Donostia-San Sebastián, Spain. [4]Saint Petersburg State University, 199034 Saint Petersburg, Russia. [5]Centro de Física de Materiales (CFM-MPC), Centro Mixto (CSIC-UPV/EHU), 20018 Donostia-San Sebastián, Spain. [6]Instituto de Nanociencia y Materiales de Aragón (INMA), CSIC-Universidad de Zaragoza, 50009 Zaragoza, Spain. [7]Present address: Department of Physics, University of Zagreb, Bijenička cesta 32, 10000 Zagreb, Croatia. ✉e-mail: evguenivladimirovich.tchoulkov@ehu.eus; mikhail.otrokov@csic.es

based on the thin films of $Mn(Bi/Sb)_2(Te/Se)_4$[32–37]. It is necessary to say that the AFM TI state of matter was for the first time theoretically proposed in 2010 by Mong, Essin, and Moore[38]. They introduced a $\mathbb{Z}_2$ topological classification of AFM insulators, provided by the $S = \Theta T_{1/2}$-symmetry, where Θ is time-reversal and $T_{1/2}$ is the primitive lattice translation. However, during almost a decade after the prediction no material satisfying these conditions was observed experimentally.

In this short review, we provide the current state-of-the-art in the research field that has emerged following the discovery of $MnBi_2Te_4$. Our aim is to offer a concise yet comprehensive overview that serves both as a quick update for researchers in the field and an accessible entry point for newcomers. We first introduce the basic properties of $MnBi_2Te_4$, followed by a discussion of the key topics, including the sample dependence of the gap in its topological surface state, native defects and their possible impact on the gap, and the surface electronic structure of $MnBi_2Te_4$ above the Néel temperature. This is followed by an exploration of the intrinsic MTIs of the $MnBi_2Te_4$ family and, eventually, the unique properties of $MnBi_2Te_4$ in the two-dimensional limit. Throughout the review, we examine the most significant and recent advancements in the field, while analyzing and highlighting its key challenges. Finally, in the outlook, we briefly discuss the exciting opportunities that the $MnBi_2Te_4$ family of compounds presents for future research and applications.

Basic properties of $MnBi_2Te_4$

The first reference to $MnBi_2Te_4$ dates back to 2013 when it was synthesized in the powder form and its structure as well as thermoelectric properties were studied[39]. It crystallizes in the trigonal $R\bar{3}m$-group structure[39–41] comprising septuple layer (SL) blocks stacked in the ABCABC fashion, in which hexagonal atomic layers follow the Te-Bi-Te-Mn-Te-Bi-Te sequence (Fig. 1a). The bonds within the blocks are ionic covalent, whereas the neighboring SLs are connected by van der Waals forces. Density functional theory (DFT) calculations coupled to the Monte Carlo simulations predict[26–28] that below $T_{Néel} = 25$ K $MnBi_2Te_4$ develops the A-type interlayer AFM structure in which the ferromagnetically-ordered Mn layers are aligned antiparallel to each other (Fig. 1a). The magnetic anisotropy energy calculations revealed the easy axis with an out-of-plane orientation of the local magnetic moments of $\pm 4.6\mu_B$. For this magnetic ground state, the insulating spectrum with the fundamental bulk bandgap of about 0.2 eV was predicted for $MnBi_2Te_4$. Having gapped spectrum and being S-symmetric due to the fortunate combination of its crystal and magnetic structures (Fig. 1a), $MnBi_2Te_4$ falls within the $\mathbb{Z}_2$ topological classification of AFM insulators[38,42]. As a result of an ab initio calculation, $\mathbb{Z}_2 = 1$ was found[26–28] thus classifying $MnBi_2Te_4$ as an AFM TI.

The combined $S = \Theta T_{1/2}$ symmetry protects the degeneracy of the Dirac point of the topological surface state of an AFM TI[38]. The surfaces that respect this symmetry are gapless, as shown in Fig. 1d, e for the $MnBi_2Te_4(10\bar{1}1)$ surface containing the $T_{1/2}$ translation. However, the S-breaking surfaces are gapped whenever there is a non-zero magnetization component perpendicular to them. Therefore the (0001) surface, which is $MnBi_2Te_4$'s natural cleavage plane, shows a band gap of several tens of meV according to the theoretical calculation (Fig. 1b, c). Large predicted magnetic gap at the Dirac point is an important characteristic making this material attractive for the QAHE and TME realization.

The magnetic and photoemission measurements performed on the bulk single crystals[26,43] and molecular-beam epitaxy grown thin films[29] confirm the AFM TI state in $MnBi_2Te_4$, which thus can be considered as the first *intrinsic* MTI. In agreement with the theoretical predictions, a long-range AFM ordering is observed in experiment[26,41,44,45], which can be identified by the λ-like shape of the magnetic susceptibility vs. temperature curve ($\chi(T)$; Fig. 2a) as well as by the presence of the characteristic spin-flop transitions in the $M(H)$ curve at H_{SF} (Fig. 2b). The Néel temperature $T_{Néel} \approx 24$–26 K is found, slightly varying from sample to sample. Subsequent neutron powder and single-crystal diffraction measurements confirmed the predicted A-type AFM ordering, as well as the out-of-plane easy axis[43,46,47]. The ARPES experiments performed on the $MnBi_2Te_4(0001)$ surface revealed the bulk band gap that hosts the linearly-dispersing topological surface state with an apparent splitting at the Dirac point[26] (see Fig. 2c).

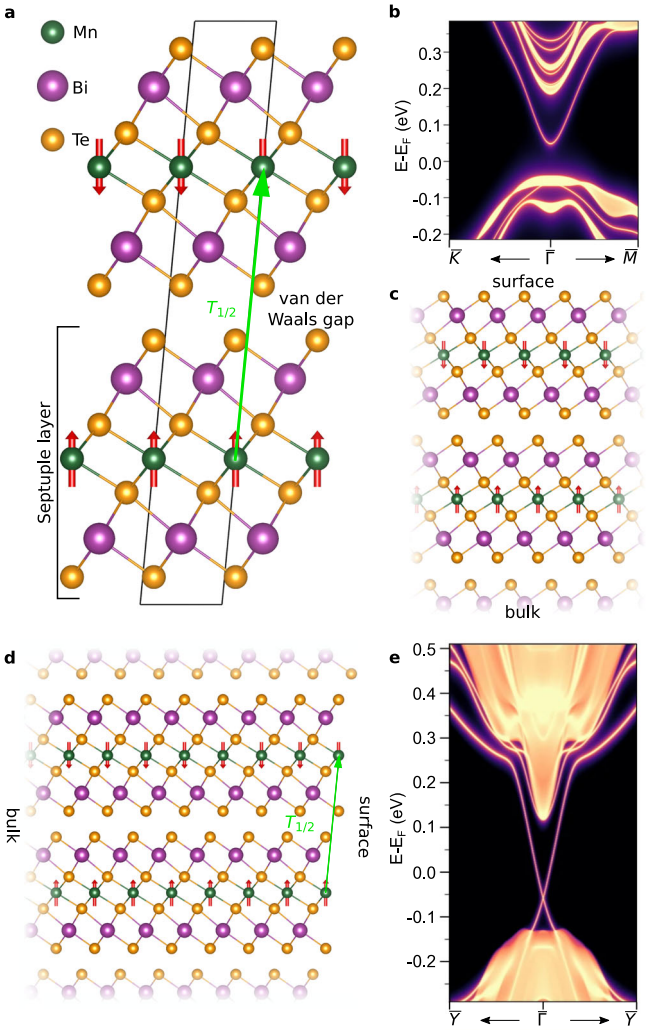

Fig. 1 | Crystal and magnetic structures as well as the calculated low-energy surface spectra of $MnBi_2Te_4$. a Crystal and magnetic structures of bulk $MnBi_2Te_4$. Red arrows denote Mn local moments, while the $T_{1/2}$ translation is shown in green. **b**, **e** Surface electronic band structures of $MnBi_2Te_4$ calculated for the (0001) (S-breaking; **c**) and for the $(10\bar{1}1)$ (S-preserving; **d**) surface terminations, respectively, using the ab-initio-based tight-binding approach. The regions with a continuous spectrum correspond to the three-dimensional bulk states projected onto a two-dimensional Brillouin zone. Observe the gapped (gapless) character of the S-breaking (S-preserving) surface. **b**, **e** are reproduced with permission from ref. 26, Copyright Springer-Nature, 2019.

Sample-dependent Dirac point gap at $MnBi_2Te_4(0001)$

The above-described experimental evidences of the AFM TI state in $MnBi_2Te_4$ were further supported by the transport experiments performed on thin films that revealed phenomena of the topological origin (see below). Very surprisingly, however, the second wave of the ARPES studies (performed with laser radiation) uncovered an unexpected behavior of the $MnBi_2Te_4$'s Dirac cone, which contradicted the one expected based on the general theory of AFM TIs[38,42], DFT calculations made for $MnBi_2Te_4$[26–28], and the results of the magnetic measurements performed on it. Namely, while the early photoemission studies[26,44,48], performed with the conventional synchrotron ARPES, reported large gaps in agreement with the theoretical predictions, a number of the following *laser*-ARPES experiments found a dramatically reduced or even vanishingly small splitting of the

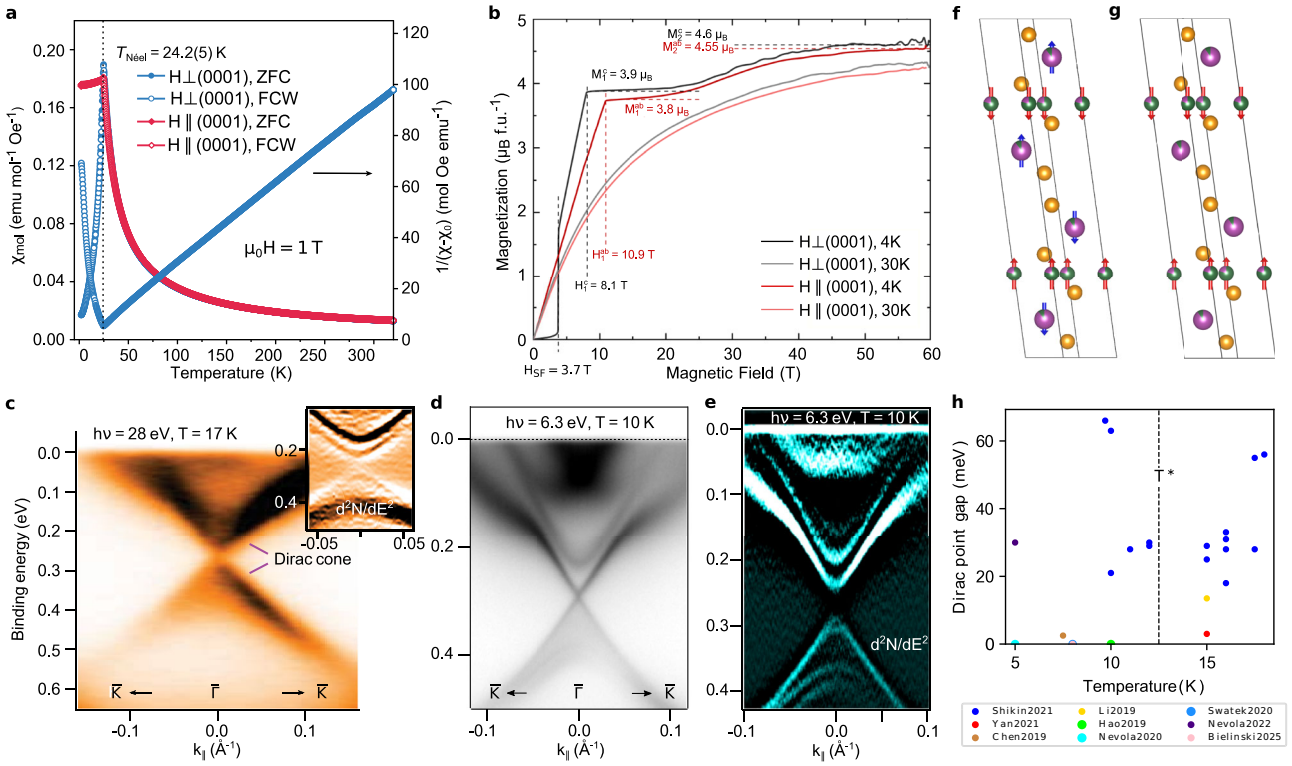

Fig. 2 | Experimentally-measured magnetic properties and surface electronic structure of $MnBi_2Te_4$. **a** Magnetic susceptibility (left axis) of $MnBi_2Te_4$ as a function of temperature measured in an external magnetic field of $\mu_0H = 1$ T in zero-field-cooled (ZFC) and field-cooled-warming (FCW) conditions, alongside the temperature-dependent reciprocal susceptibility (right axis) for $H\perp(0001)$. **b** High-field magnetization data of $MnBi_2Te_4$ at 4 and 30 K with the field applied either along the *c* axis or in the *ab* plane. H_{SF} denotes the spin-flop magnetic field. Dispersion of the topological surface state of $MnBi_2Te_4$(0001) measured with (**c**) a conventional synchrotron ARPES (photon energy $h\nu = 28$ eV, $T = 17$ K) and (**d**, **e**) laser-ARPES ($h\nu = 6.3$ eV, $T = 10$ K). In (**d**, **e**) the data acquired on two samples synthesized by different groups are shown. In (**e**) the second derivative data, $d^2N(E)/dE^2$, are presented. Note the reduced intensity at the expected Dirac point position in (**c**), indicative of the gap, which is also seen in (**e**), while, in contrast, the Dirac cone is gapless in (**d**). In the inset to (**c**), the second derivative ($d^2N(E)/dE^2$) of the data taken with a more bulk sensitive photons ($h\nu = 9$ eV, $T = 17$ K) is presented, where the bulk valence and conduction bands, separated by a gap of about 0.2 eV[190], can be seen. Magnetic structure of $MnBi_2Te_4$ below (**f**) and above (**g**) T^*, see text for the explanation. Note that the intermixing levels are intentionally enhanced for the visualization purposes. **h** Compilation of the literature data on the Dirac point gap size, as measured by different groups using laser-ARPES. Only the data reported for $T < T_{Néel}$ are shown. Note that Shikin et al.[58] report data on 15 different $MnBi_2Te_4$ samples, as shown by blue circles. **a**, **c** are reproduced with permission from ref. 26, Copyright Springer-Nature, 2019. **b** is reproduced with permission from ref. 45, Copyright American Physical Society, 2021. **d** is reproduced from ref. 49. **e** is reproduced with permission from ref. 58, Copyright American Physical Society, 2021.

$MnBi_2Te_4$ Dirac cone[49–52] (Fig. 2d). Figure 2h summarizes all the available data on the Dirac point gap measured by laser-ARPES[49–51,53–58]. It can be seen that in the currently available $MnBi_2Te_4$ samples the Dirac point gap can acquire an arbitrary value between a few and several tens of meV. An example of the laser-ARPES spectrum showing a large Dirac point gap is presented in Fig. 2e.

Several scenarios have been proposed to account for this unexpected behavior[49,52,59–62]. On the one hand, possible changes of magnetism near the $MnBi_2Te_4$ surface have been suggested, such as near-surface magnetic dead layer[60] or a deviation of the magnetic structure or easy magnetization axis from those in bulk[49,61]. Recent scanning tunneling spectroscopy study reports asymmetric quasiparticle interference pattern of the topological surface state close to the Dirac point[63], which would be in line with the presence of the in-plane magnetization component at the $MnBi_2Te_4$(0001) surface. However, this is corroborated by neither the X-ray magnetic circular dichroism measurements[26,52] nor magnetic force microscopy experiments[64], that provide evidences of the persistence of uniaxial A-type AFM order up to the surface layers of the $MnBi_2Te_4$ single crystals.

On the other hand, possible structural factors have been considered, such as surface collapse during the mechanical exfoliation[59] or expansion of the first van der Waals gap[52] (i.e., the increase of the spacing that separates the surface SL from the subsurface one). However, the former was only observed during the exfoliation in an inert gas environment and never in the ultra-high vacuum, while the latter needs to be quite large (about 15 %) to close the Dirac point gap, but such expansions have not been observed in experiment[65,66].

Mn-Bi intermixing and its possible impact on the Dirac point gap

Latest theoretical studies discuss Mn-Bi intermixing as the most likely cause of the Dirac point gap reduction in $MnBi_2Te_4$[66,67]. To discuss the latter, let us first review the effect of the Mn-Bi intermixing on the $MnBi_2Te_4$ magnetic structure. High-field magnetization study[45] revealed that above the first magnetization plateau at $\mu_0H_1^c \approx 8$ T (Fig. 2b) the magnetization smoothly increases further and eventually saturates to $M_2^c \approx 4.6\mu_B$/f.u. near 50 T. The reason for such evolution of $M(H)$ from the first (M_1^c) to the second (M_2^c) plateau has been suggested a spin flip of Mn ions residing on the Bi site (Mn_{Bi}). In other words, in the ground state, each $MnBi_2Te_4$ SL block is "ferrimagnetic" (Fig. 2f), in which the local moments of the Mn_{Bi} atoms are coupled antiparallel to those of the central Mn layer, as has initially been found for $MnSb_2Te_4$ by neutron diffraction measurements[68].

Going back to the discussion of possible mechanisms of the Dirac point gap reduction, ref. 66 argues that it is the opposite magnetization of the Mn_{Bi} antisites (with respect to the central Mn layer) that causes the Dirac point gap reduction. This happens because the magnetic antisites are introduced exactly in the regions of the topological surface state predominant localization in the real space, which is around the Bi layers. Thus the oppositely directed magnetic moments of the antisites can

effectively counteract the magnetic effect of the central layer Mn atoms, around which the topological surface state weight is small. As illustrated by DFT calculations[66], even a moderate amount of the Mn_{Bi} antisites may result in a significant reduction of the Dirac point gap or even in its almost complete shrinking. In contrast, according to the DFT results in ref. 67, the Mn-Bi intermixing "pushes" the topological surface state towards the subsurface SL, whereupon the magnetic gap is diminished heavily due to the AFM alignment between the surface and subsurface SL blocks. It should, however, be noted that both DFT studies[66,67] introduce the intermixing only in the topmost SL of the slabs used, while the other SLs are pristine. Thus, the calculations using more realistic structural models are needed to clarify which mechanism actually takes place in the experimental samples.

Recent scanning tunneling spectroscopy studies[69,70] of the Dirac point gap behavior in the molecular-beam epitaxy grown thin $MnBi_2Te_4$ films reveal the gap fluctuation across the surface. At that, the gap values ranging between 0 (gapless) and 70 meV have been measured. These studies differ, however, as far as the correlation of the gap size with the point defects distribution is concerned. While ref. 69 reveals that the gap is absent (present) in the regions with a high (low) concentration of Mn_{Bi} defects, ref. 70 concludes that the gap size is uncorrelated to individual Mn_{Bi} and Bi_{Mn} defects. Instead, the Dirac point gap fluctuation appears to take place on the nanometer scale. Remarkably, application of the external magnetic field of about 1 T significantly reduces the gap fluctuations and leads to the increase of the average gap from 26.3 meV to 44 meV[70]. The sensitivity of the Dirac point gap to the moderate magnetic field could be consistent with a deviation of the near-surface magnetic structures from the bulk one, as mentioned above[63].

In this context, an important comment should be made. Out of all defects generated by the Mn-Bi intermixing, only the Mn_{Bi} antisites from the first Bi layer (i.e., the second atomic layer from the surface) are clearly seen in the scanning tunneling microscopy. Imaging of the Bi_{Mn} defects that lie in the fourth atomic layer from the surface is already quite difficult[66,70,71]. As far as the the sixth atomic layer Mn_{Bi} defects are concerned, to the best of our knowledge, no feature that would be clearly attributed to them has been reported in the scanning tunneling microscopy studies. These features should undoubtedly be faint and, because their extension should be about several lattice parameters as a minimum, may laterally overlap with each other as well as with those from defects in other layers, making them hardly distinguishable. Nevertheless imaging of the sixth layer Mn_{Bi} antisites is highly desirable since, according to the DFT calculations[66], their negative effect on the Dirac point gap is expected to be much stronger than that of the second layer Mn_{Bi}. This is because the sixth atomic layer (again, counting from the surface) carries a much larger weight of the topological surface state in the real space[66].

Latest experimental data shed more light onto the magnetism of the $MnBi_2Te_4$ family, which might be relevant in the context of the Dirac point gap issue. The nuclear magnetic resonance and muon spin spectroscopy measurements not only directly confirm the ferrimagnetic structure of the $MnBi_2Te_4$ SLs (and those of $MnBi_2Te_4 \cdot nBi_2Te_3$ discussed below), but also reveal that the static magnetic moment of the Mn_{Bi} antisite sublattice disappears at $T^* < T_{Néel}$, T^* being equal to 12.5 K in the $MnBi_2Te_4$ case[72], i.e., below (above) T^* the Mn_{Bi} sublattice is ordered (paramagnetic), as shown in Fig. 2f, g. It would be very interesting to explore the Dirac point gap behavior across T^*, given that one of the proposed scenarios[66] attributes the gap reduction to the AFM coupling between the Mn_{Bi} and Mn_{Mn} sublattices when both of them are ordered (i.e., below T^*). The existing temperature-dependent photoemission data[58] do not elucidate this behavior since the lowest measurement temperature (~10 K) is too close to the expected T^*. Note that for the samples studied in ref. 58 T^* are unknown. It is reasonable to assume that T^* can slightly vary from sample to sample (likely depending on the degree of intermixing), pretty much as the Néel temperature of $MnBi_2Te_4$ varies within the 24–26 K range[66,72]. Taking also into account the instrument error in the temperature determination and the temperature step of about 1.7 K in ref. 58, it is difficult to draw conclusions about the Dirac point gap behavior across T^* from that experiment. The compilation of the laser-ARPES results shown in Fig. 2h does not clarify this issue either, since the measurements have been performed by different groups on different samples. Meanwhile, using time- and angle-resolved photoemission spectroscopy, it has been found that opposite helicities of mid-infrared circularly polarized light result in substantially different Dirac mass gaps in the $MnBi_2Te_4$ topological surface state below T^* (at 8 K), despite the equilibrium Dirac cone being massless[57].

$MnBi_2Te_4$ surface electronic structure above $T_{Néel}$

At this point, the surface electronic structure of $MnBi_2Te_4$ above the Néel temperature should also be discussed. A number of ARPES studies, both synchrotron[26,44,48] and laser based[26,50,52,58,73], in which the Dirac point gap has been detected in the AFM state, reported its persistence in the paramagnetic (PM) phase, similarly to what was previously observed for the magnetically-doped Bi_2Se_3[74,75]. At that, in majority of the cases, $MnBi_2Te_4$'s Dirac point gap size in the AFM and PM phases is practically the same, with only one laser-ARPES study reporting a ~40% reduction of the gap (from 65 to 40 meV) upon heating from below $T_{Néel}$ up to 35 K[58]. Such a behavior challenges the idea of the magnetically induced gap, as the latter should disappear at or just above the critical point, pretty much as it happens with the exchange splitting of the first bulk conduction and valence bands observed for $MnBi_2Te_4$[51,73]. However, in $MnBi_2Te_4$ the persistence of the Dirac point gap could be caused by strong short range order effects that exist up to about 60 K, as observed by electron spin resonance, as well as ferromagnetic and AFM resonance experiments[26,76,77]. The measured magnetization data[45], revealing that $MnBi_2Te_4$ is not in the PM limit even at $T \approx 50$ K, support the latter observations. Such a behavior is also consistent with the strong spin fluctuation-driven spin scattering above $T_{Néel}$ found in a previous magneto-transport study of $MnBi_2Te_4$ in ref. 44. Beyond 50–60 K, an unprecedentedly large anisotropy of the Mn spin relaxation rate in the PM state of $MnBi_2Te_4$[26,76] may give rise to an instantaneous (on the timescale of electron spin resonance) out-of-plane magnetic field at the surface, preventing the gap from closing *on the much faster timescale of the ARPES experiment*.

MTIs of the $MnBi_2Te_4$ family

In spite of the Dirac point gap puzzle, $MnBi_2Te_4$ has attracted significant interest of the research community due to its unusual and highly tunable properties. Multiple tuning knobs, not only extrinsic such as magnetic field, pressure, and temperature, but also intrinsic such as Mn-Mn interlayer distance, chemical composition, and defect engineering, can be used to realize various magnetic and topological states in $MnBi_2Te_4$ or systems on its basis. For example, pnictogen or chalcogen substitutions and Mn/Bi/Te stoichiometry alternations give rise to such materials as $Mn(Bi_{1-x}Sb_x)_2Te_4$, $MnSb_2Te_4$, $MnBi_2Se_4$, or $Mn_2Bi_2Te_5$, whose magnetic and topological properties were studied both theoretically and experimentally[78–86]. In particular, $MnBi_2Se_4$, while being AFM TI with the same A-type structure as $MnBi_2Te_4$, displays staggered magnetization within the Mn plane[82], which may give rise to the one-dimensional topologically-protected flat bands pinned to the magnetic domain walls at its surface, as predicted by theory[87]. Incidentally, recent experimental and theoretical X-ray magnetic circular dichroism study has revealed that the Mn_{Bi} antisites in the SLs of the $MnBi_2Se_4/Bi_2Se_3$ heterostructure are coupled ferromagnetically to the central Mn plane of the SL[88], in a stark contrast to the $MnBi_2Te_4$ case, where this coupling is AFM[45,72]. This striking difference has been attributed to a stronger hybridization of the Mn_{Bi}-*d* states with the Se-*p* states in $MnBi_2Se_4$ as compared to that with Te-*p* in $MnBi_2Te_4$, due to the shorter bondlength in the former. Another material with the 1-2-4 stoichiometry, $MnSb_2Te_4$, seems to be on the verge of the topological phase transition, as the DFT calculations reveal a strong sensitivity of its topology to the crystal structure details[27,68,89–91], while the available experimental data are contradictory[80,92] and further studies are needed. Mixing Bi and Sb on the pnictogen sublattice to create $Mn(Bi_{1-x}Sb_x)_2Te_4$, enables realization of the Weyl semimetal state

in the fully polarized ferromagnetic (FM) state[27,28], which was experimentally achieved by applying a sufficiently strong external magnetic field that overcomes the AFM interlayer exchange coupling[81,93]. Ge-, Sn-, and Pb-doped $MnBi_2Te_4$ single crystals were also synthesized[94–96], showing peculiar topological phase transition[97].

Furthermore, the van der Waals nature of $MnBi_2Te_4$ enables "intercalating" the adjacent SLs with Bi_2Te_3 quintuple layers, resulting in the $MnBi_2Te_4 \cdot nBi_2Te_3$ family of compounds ($n = 1$ for $MnBi_4Te_7$, $n = 2$ for $MnBi_6Te_{10}$, and so on, up to $n = 6$)[40,98–100]. The increasing distance between the SLs progressively weakens the interlayer exchange coupling with an increasing n[101], which enables an effective tuning of the magnetic structure by moderate magnetic fields[102–107], or hydrostatic pressure[108], driving these compounds from the AFM to the FM state. Overall, apart from the 3D AFM TI state, under different conditions $MnBi_2Te_4 \cdot nBi_2Te_3$ materials may show topological crystalline insulator state[102] as well as higher order topologies such as Möbius[109] or $\mathbb{Z}_4$-axion[109–112] insulators, 2D AFM second order TI[113] or topological superconductor[114] states.

Magnetic antisite defects in the materials of the $MnBi_2Te_4$ family are lately in the center of attention not only because of their possible negative impact on the Dirac point gap but also thanks to their strong influence on the magnetic and electronic structure: they are exploited as an effective tuning knob to purposely modify the latter[68,115,116]. The cation intermixing between the manganese and pnictogen crystallographic sites is favored by closeness of their ionic radii. This is especially true for $MnSb_2Te_4$ that supports up to ~40% of Sb atoms in the Mn layer, while, in turn, up to ~15% of each Sb layer is occupied by Mn atoms[68]. For $MnBi_2Te_4$ the intermixing levels are roughly three times lower[41]. Strong intermixing in $MnSb_2Te_4$ promotes the FM coupling between the adjacent SLs[117]. At that, the magnetic transition temperature jumps from $T_{Néel} = 19$ K in the AFM-like bulk $MnSb_2Te_4$ single crystals[68] to $T_{Curie} = 73$ K in the FM-like ones[118], which is achieved by varying the growth conditions with a certain degree of control[68]. According to the DFT calculations, while a moderate Mn-Sb intermixing promotes the Weyl semimetal state due to the change of the interblock coupling to FM, its increase eventually renders $MnSb_2Te_4$ gapped and topologically trivial[68,80]. Apart from $MnSb_2Te_4$, the interlayer coupling can also become truly FM in the Sb-doped $MnBi_2Te_4 \cdot nBi_2Te_3$[119,120] and even in $MnBi_6Te_{10}$, in the latter case via the Mn-Bi defects engineering under appropriate growth conditions[115,116], which may help to achieve an FM axion insulator state[109,110].

$MnBi_2Te_4$ in the two-dimensional limit

$MnBi_2Te_4$ properties in the two-dimensional limit are exciting, too. Magnetism and topology of thin $MnBi_2Te_4$ films are thickness-dependent, while different symmetries in even- and odd-SL films lead to distinct phenomena[28–30,121,122]. The films with odd (even) number of SLs are uncompensated (fully compensated) interlayer antiferromagnets, which break (preserve) the $P\Theta$ symmetry[28], P being inversion. In the films made of even number of blocks, the $P\Theta$ symmetry leads to the Chern number $C = 0$, while a $C \neq 0$ is allowed in the films with the odd number. According to DFT calculations[28,30], while the one-SL-thick film is topologically trivial, the 5- and 7-SL-thick ones are QAH insulators with $C = 1$ (the predictions on the 3-SL-thick film are contradictory[28,30]). On the other hand, the 2-, 4-, and 6-SL-thick films were predicted to show the so-called zero plateau QAH state. The importance of the zero plateau QAH state is that it can be a suitable platform for realization of the TME, characteristic of the axion insulator phase[123].

Soon after the theoretical predictions[28,30], the zero plateau QAH state has been observed experimentally in the $MnBi_2Te_4$ thin flakes made of *even* number of SLs[124], see Fig. 3a, b. Previously, this state of matter was being sought for in the FM1/TI/FM2 QAH heterostructures, where a relatively thick TI spacer enables magnetization reversal of the individual FM layers that have different coercivities, leading to the overall AFM alignment and, consequently, to a zero plateau QAH state[125,126]. In theory, the $MnBi_2Te_4$ thin films made of even number of SLs realize this state intrinsically, i.e., without the need of magnetic field application. In practice, however, a magnetic field of about 8 T is applied and swiped to 0 T to prepare a single-domain AFM state with the desired orientation of the topmost SL magnetization, up or down[127,128]. It should also be noted that a thickness of 6 SLs[124] is likely insufficient for the TME to be quantized because of the finite-size effect[123,129,130], however, it should become fully quantized upon increasing the film thicknesses towards the 3D limit.

Further experimental work not only confirms the zero plateau QAH state in 2D even-layered $MnBi_2Te_4$,[127,131] but also reveals a series of other novel phenomena[127,128,131–133]. One of them is the layer Hall effect, in which the electrons from the top and bottom layers of the film spontaneously deflect in the opposite directions, which is due to the opposite signs of the Berry curvature[127,134]. Observation of the effect is enabled by applying external electric field that breaks $P\Theta$, leading to the emergence of a finite anomalous Hall effect (AHE), which is dominated by either top or bottom layer, depending on the field direction. Moreover, the opposite sign of the Berry curvature of the top and bottom surfaces is responsible for the appearance of the axion (i.e., surface[135]) contribution to the optical magnetoelectric coupling, as recently predicted[136] and observed for the 2D even-layered $MnBi_2Te_4$[131]. This effect enables optical control of the AFM order, i.e., selective stabilization of one or another AFM domain (up-down or down-up) by the circularly polarized light with either opposite helicity or different frequencies that couples differently to the opposite AFM domains.

Another unusual phenomenon recently witnessed in the thin $MnBi_2Te_4$ flakes with even number of blocks is the second-order nonlinear AHE[132,133], in which an alternating current (a.c.) with frequency ω induces an a.c. Hall voltage with frequency 2ω. In this case, the Berry curvature is not the origin of the effect, since it is equal to zero as dictated by the $P\Theta$ symmetry. Instead, the effect is generated by the quantum metric of the gapped $MnBi_2Te_4$ Dirac cone[132,133]. More recently, third-order nonlinear Hall effect in both longitudinal and transverse directions in thick $MnBi_2Te_4$ flakes has been reported[137]. The longitudinal third-harmonic response $V_{xx}^{3\omega}$ has been found to appear due to the quantum metric quadrupole, while the transverse response $V_{xy}^{3\omega}$ due to the Berry curvature quadrupole. Thus, $MnBi_2Te_4$ enables probing both the real and the imaginary part of the quantum geometric tensor of the Bloch states in transport experiments.

As for the predicted QAHE (i.e., the quantum Hall effect (QHE) in zero magnetic field), its observation in the *odd-layered* 2D $MnBi_2Te_4$ has proven challenging. In fact, initially $MnBi_2Te_4$ has shown the quantized Hall effect only under external magnetic field[138,139], but not without it (note that refs. 138,139 are preprint versions of[124,140]). The field has been used to overcome the AFM interlayer exchange coupling thus forcing the FM state (Fig. 3a), while the gate bias is employed to find the charge neutrality point, which in $MnBi_2Te_4$ should correspond to the gap in the Dirac point. At the magnetic fields used (about 9 T), the magnetic moments of the Mn_{Bi} antisites are most likely still ordered oppositely to those of the central Mn layer[45]. However, this does not suppress the quantized Hall effect. In fact, the effect can be observed already in the canted AFM state, just after the spin-flop transition[141]. Upon further increase of the magnetic field strength, the canted AFM state transforms into the forced FM state with the QHE observed continuously. The absence of the free carriers at the Fermi level translates into the absence of Landau levels (LLs) in spite of the field application (in contrast to the conventional QHE[142]) and the QHE stems from the nontrivial topology of the $MnBi_2Te_4$'s band structure in the forced FM state. Envisioned by theory[28,30], this $C = 1$ QHE without LL formation in $MnBi_2Te_4$ has been repeatedly observed in experiment by different groups to this date[124,127,140,141,143–148], with a reasonable quantization persisting up to 30 K[143]. Worth mentioning as well is the $C = 2$ state without LLs that onsets in the flakes thicker than 9 SLs of $MnBi_2Te_4$ under external magnetic field and persists up to about 10 K[91,143]. Finally, the conventional QHE *with* LLs[142] can be observed in the $MnBi_2Te_4$ flakes too[140], which, apart from a rather strong magnetic field, requires increasing the carrier concentration by applying bias voltage.

The zero-field QAHE has been observed in the 5-SL-thick film[140], as shown in Fig. 3c, d. However, further advances in this direction have been slow, likely due to the difficulties in obtaining high-quality samples with

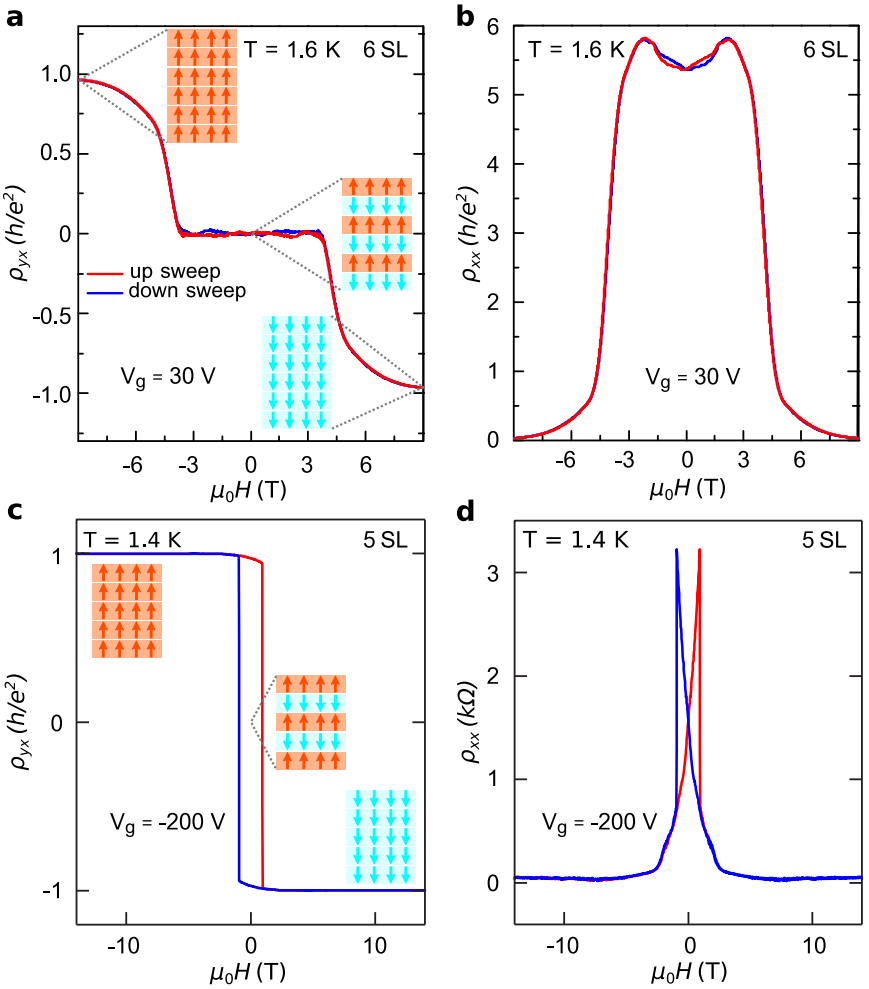

Fig. 3 | Q(A)HE and its zero-plateau in $MnBi_2Te_4$ flakes. Magnetic field driven transition from the zero-plateau QAH state (around the zero field, corresponding to $\rho_{yx} = 0$ (**a**) and very large ρ_{xx} (**b**)) to the Chern insulator with QHE (at ± 9 T, with the nearly quantized $\rho_{yx} \approx \mp h/e^2$ (**a**) and vanishing ρ_{xx} (**b**)) measured in a 6-SL-thick $MnBi_2Te_4$ flake at $T = 1.6$ K. The measurement is performed using the back-gate voltage $V_g = 30$ V, which corresponds to the charge neutrality point when the Fermi level lies within the surface state gap. Quantum anomalous Hall effect in a 5-SL-thick $MnBi_2Te_4$ flake illustrated by the magnetic field dependence of ρ_{yx} (**c**) and ρ_{xx} (**d**), measured at $T = 1.4$ K and $V_g = -200$ V. At $\mu_0 H = 0$ T, ρ_{yx} reaches $0.97h/e^2$, while ρ_{xx} is suppressed ($0.061h/e^2$), evidencing the QAHE. The insets in (**a**, **c**) schematically show the magnetic structure of the flakes at zero and high fields. **a**, **b** are reproduced with permission from ref. 124, Copyright Springer-Nature, 2020. **c**, **d** are reproduced with permission from ref. 140, Copyright AAAS, 2020.

reduced levels of the Mn-Bi intermixing, although the device fabrication process seems to introduce further complications[59,149]. A valuable insight into the quantized transport of the odd-layered $MnBi_2Te_4$ flakes has been provided by scanning superconducting quantum interference device microscopy used to image their current distribution[150]. A chiral edge current in the 7-SL-thick flake at zero magnetic field has been observed, confirming its topological nature. However, the finite bulk conduction and edge-bulk scattering have been found to undermine the transport quantization. This is consistent with the scanning tunneling spectroscopy data that image both the edge state of the 5-SL-thick molecular-beam epitaxy grown $MnBi_2Te_4$ film and its coupling to the gapless two-dimensional bulk regions arising from band gap fluctuations[70]. However, very recently, a new procedure in the device preparation, consisting in depositing an AlO_x layer on the $MnBi_2Te_4$ flake surface prior to nano-fabrication, has enabled a significant improvement of the AHE phase quality, with the true zero-field QAHE achieved in few samples[151,152]. Applying a hydrostatic pressure also allowed approaching the QAHE regime in 2D $MnBi_2Te_4$[153].

Recently, an intriguing behavior has been reported for the molecular-beam epitaxy grown 5 SL $MnBi_2Te_4$ film showing the QHE without LLs in the forced FM state. Tuning the gate voltage through the QHE region up until the quantization breakdown, when ρ_{yx} is no longer equal to h/e^2, and then switching the field off (for the material to adopt the AFM state) leads to reappearance of a nearly quantized ρ_{yx} plateau of $\approx h/e^2$[154]. This happens for the Fermi level located in the valence band and not in the global gap. Despite the latter, as well as nonzero $\rho_{xx} \approx 0.85h/e^2$, this state shows $\tan(\theta_H)$ vs. T behavior ($\theta_H = \rho_{yx}/\rho_{xx}$ is the Hall angle), which is more similar to that of the zero-field QAHE in $MnBi_2Te_4$[140,153], rather than the insulating zero field state of the very same epitaxial film at the charge neutrality point. The appearance of this phase, dubbed "reentrant QAHE", has been attributed to the exchange-induced Berry curvature splitting and disorder-induced Anderson localization[154,155].

Outlook

Let us now briefly outline other exciting phenomena that compounds of the $MnBi_2Te_4$ family have been reported to (or may potentially) host. While we do not delve into details—an undoubtedly worthwhile endeavor that lies beyond the scope of this short review—we nevertheless highlight these intriguing studies as a roadmap for future research. Apart from the above-described variants of the Hall effect, the compounds of the $MnBi_2Te_4$-family were reported to show the QAHE in the 3D limit[156], as well as the topological[157,158] and planar Hall effects[159]. Pending the observation are the predicted half-integer QHE[38], Θ-breaking quantum spin Hall effect[160], and its "hinged" version[161], interfacial crystal Hall effect[162], orbital Hall effect[163], as well the quantized version of the layer Hall effect[164]. Besides, $MnBi_2Te_4$-based systems could be a platform for novel topological heterostructures[32,34,160,165–169], anomalous Nernst effect[170], high-Chern number phases[171], skyrmions[172] (in particular, coexisting with QAHE, which may generate novel topological phases[173]), and Majorana fermions[174]. Recent studies are seeking to induce superconductivity in $MnBi_2Te_4$ either via proximitizing it to a conventional superconductor $NbSe_2$[175] or via interfacing $MnBi_2Te_4$ film to that of a non-superconducting AFM material FeTe[176].

Novel device proposals based on the systems of the $MnBi_2Te_4$-family have already been put forward[177,178], such as rectifiers, spin filters, negative differential resistive devices, photoelectric sensors, photovoltaic, magneto-optoelectronic devices. The layer Hall effect makes $MnBi_2Te_4$ a potential platform to explore the 'layertronics' to encode, process, and store

information[179], while the recently observed AFM diode effect[128,133] may enable a field-effect transistor and harvesting of wireless electromagnetic energy[128]. Quantum computing and sensing applications have also been envisioned[180,181].

It should be said, however, that this research field is only in its infancy, and many results are still to be confirmed and understood, while many new exciting discoveries are likely to come soon. The most important task appears to be achieving an exhaustive explanation of the unexpected behavior of the $MnBi_2Te_4$ topological surface state gap and further detailed studies are needed. However, since the Mn-Bi intermixing seems to be detrimental in this sense, suppressing it could hopefully allow getting rid of the Dirac point gap issue in $MnBi_2Te_4$. Steps in this direction are being taken currently[69,145,148,182,183]. Achieving this objective might translate into the improved quality of the experimental samples and, hence, to an observation of a plethora of phenomena and states of matter the $MnBi_2Te_4$ family is capable of hosting. In particular, it could enable realization of the robust intrinsic QAHE in $MnBi_2Te_4$, whose observation temperature may be expected to jump significantly above the currently reported 1.5 K[140].

For further detailed reading on the intrinsic MTIs of the $MnBi_2Te_4$-family we recommend the following review articles[183–187].

We have recently learned of the experimental observation of the topological Anderson Chern insulator phase in the $[MnBi_2Te_4]_{1SL}/[Bi_2Te_3]_{1QL}$ heterostructure (where QL stands for quintuple layer), as reported in ref. 188. More recently, the observation of a dynamical axion quasiparticle, i.e., a solid-state incarnation of the high-energy axion particle, has been reported in the 2D $MnBi_2Te_4$. This discovery may ultimately pave the way for the experimental detection of the elusive axion particle[189].

Received: 1 July 2024; Accepted: 28 March 2025;
Published online: 30 April 2025

References

1. Hasan, M. Z. & Kane, C. L. Colloquium: topological insulators. *Rev. Mod. Phys.* **82**, 3045–3067 (2010).
2. Qi, X.-L. & Zhang, S.-C. Topological insulators and superconductors. *Rev. Mod. Phys.* **83**, 1057–1110 (2011).
3. Haldane, F. D. M. Model for a quantum Hall effect without Landau levels: condensed-matter realization of the "parity anomaly". *Phys. Rev. Lett.* **61**, 2015–2018 (1988). This paper proposes the concept of the quantum Hall effect in the absence of an external magnetic field.
4. Liu, C.-X., Qi, X.-L., Dai, X., Fang, Z. & Zhang, S.-C. Quantum anomalous Hall effect in $Hg_{1-y}Mn_yTe$ quantum wells. *Phys. Rev. Lett.* **101**, 146802 (2008).
5. Yu, R. et al. Quantized anomalous Hall effect in magnetic topological insulators. *Science* **329**, 61–64 (2010).
6. Chang, C.-Z., Liu, C.-X. & MacDonald, A. H. Colloquium: quantum anomalous Hall effect. *Rev. Mod. Phys.* **95**, 011002 (2023).
7. Shapiro, J. The bulk-edge correspondence in three simple cases. *Rev. Math. Phys.* **32**, 2030003 (2020).
8. Zhang, S. & Zhang, X. Electrical and optical devices incorporating topological materials including topological insulators. US Patent 9,024,415 (2015).
9. Qi, X.-L., Hughes, T. L. & Zhang, S.-C. Topological field theory of time-reversal invariant insulators. *Phys. Rev. B* **78**, 195424 (2008).
10. Mahon, P. T., Lei, C. & MacDonald, A. H. Symmetry, topology, and geometry: the many faces of the topological magnetoelectric effect. *Phys. Rev. Res.* **6**, 023289 (2024).
11. Essin, A. M., Moore, J. E. & Vanderbilt, D. Magnetoelectric polarizability and axion electrodynamics in crystalline insulators. *Phys. Rev. Lett.* **102**, 146805 (2009).
12. Sekine, A. & Nomura, K. Axion electrodynamics in topological materials. *J. Appl. Phys.* **129**, 141101 (2021).
13. Tse, W.-K. & MacDonald, A. H. Giant magneto-optical Kerr effect and universal Faraday effect in thin-film topological insulators. *Phys. Rev. Lett.* **105**, 057401 (2010).
14. Chang, C.-Z. et al. Experimental observation of the quantum anomalous Hall effect in a magnetic topological insulator. *Science* **340**, 167–170 (2013). This paper reports the first observation of the quantum anomalous Hall effect.
15. Checkelsky, J. G. et al. Trajectory of the anomalous Hall effect towards the quantized state in a ferromagnetic topological insulator. *Nat. Phys.* **10**, 731–736 (2014).
16. Okazaki, Y. et al. Quantum anomalous Hall effect with a permanent magnet defines a quantum resistance standard. *Nat. Phys.* **18**, 25–29 (2022).
17. Serlin, M. et al. Intrinsic quantized anomalous Hall effect in a moiré heterostructure. *Science* **367**, 900–903 (2020). This paper reports the realization of the quantum anomalous Hall effect in twisted bilayer graphene.
18. Li, T. et al. Quantum anomalous Hall effect from intertwined moiré bands. *Nature* **600**, 641–646 (2021). This paper reports the realization of the quantum anomalous Hall effect in transition metal dichalcogenide moiré heterobilayers.
19. Mogi, M. et al. Experimental signature of the parity anomaly in a semi-magnetic topological insulator. *Nat. Phys.* **18**, 390–394 (2022). This paper reports the observation of the half-integer quantization of Hall conductance in a magnetic topological insulator heterostructure.
20. Lee, I. et al. Imaging Dirac-mass disorder from magnetic dopant atoms in the ferromagnetic topological insulator $Cr_x(Bi_{0.1}Sb_{0.9})_{2-x}Te_3$. *Proc. Natl. Acad. Sci. USA* **112**, 1316–1321 (2015).
21. Lachman, E. O. et al. Visualization of superparamagnetic dynamics in magnetic topological insulators. *Sci. Adv.* **1**, e1500740 (2015).
22. Krieger, J. A. et al. Spectroscopic perspective on the interplay between electronic and magnetic properties of magnetically doped topological insulators. *Phys. Rev. B* **96**, 184402 (2017).
23. Mogi, M. et al. Magnetic modulation doping in topological insulators toward higher-temperature quantum anomalous Hall effect. *Appl. Phys. Lett*. **107**, 182401 (2015).
24. Li, W. et al. Origin of the low critical observing temperature of the quantum anomalous Hall effect in V-doped $(Bi,Sb)_2Te_3$ film. *Sci. Rep.* **6**, 32732 (2016).
25. Kim, C. K., Denlinger, J. D., Kundu, A. K., Gu, G. & Valla, T. Absence of a Dirac gap in ferromagnetic $Cr_x(Bi_{0.1}Sb_{0.9})_{2-x}Te_3$. *J. Appl. Phys*. **129**, 083902 (2021).
26. Otrokov, M. M. et al. Prediction and observation of an antiferromagnetic topological insulator. *Nature* **576**, 416–422 (2019). This paper predicts the intrinsic antiferromagnetic topological insulator $MnBi_2Te_4$ and experimentally confirms it for the bulk crystals.
27. Zhang, D. et al. Topological axion states in the magnetic insulator $MnBi_2Te_4$ with the quantized magnetoelectric effect. *Phys. Rev. Lett.* **122**, 206401 (2019). This paper predicts the antiferromagnetic topological insulator state in $MnBi_2Te_4$.
28. Li, J. et al. Intrinsic magnetic topological insulators in van der Waals layered $MnBi_2Te_4$-family materials. *Sci. Adv.* **5**, eaaw5685 (2019). This paper predicts the antiferromagnetic topological insulator state in $MnBi_2Te_4$.
29. Gong, Y. et al. Experimental realization of an intrinsic magnetic topological insulator. *Chin. Phys. Lett.* **36**, 076801 (2019). This paper reports observation of the intrinsic antiferromagnetic topological insulator state in the $MnBi_2Te_4$ molecular-beam epitaxy grown ultrathin films.
30. Otrokov, M. M. et al. Unique thickness-dependent properties of the van der Waals interlayer antiferromagnet $MnBi_2Te_4$ films. *Phys. Rev. Lett.* **122**, 107202 (2019). This paper predicts the quantum anomalous Hall effect and its zero-plateau state in the 2D limit of $MnBi_2Te_4$.
31. Rienks, E. et al. Large magnetic gap at the Dirac point in $Bi_2Te_3/MnBi_2Te_4$ heterostructures. *Nature* **576**, 423–428 (2019).

32. Otrokov, M. M. et al. Highly-ordered wide bandgap materials for quantized anomalous Hall and magnetoelectric effects. *2D Mater.* **4**, 025082 (2017).
33. Otrokov, M. M. et al. Magnetic extension as an efficient method for realizing the quantum anomalous Hall state in topological insulators. *JETP Lett.* **105**, 297–302 (2017).
34. Hirahara, T. et al. Large-gap magnetic topological heterostructure formed by subsurface incorporation of a ferromagnetic layer. *Nano Lett.* **17**, 3493–3500 (2017).
35. Eremeev, S. V., Otrokov, M. M. & Chulkov, E. V. Competing rhombohedral and monoclinic crystal structures in $MnPn_2Ch_4$ compounds: an ab-initio study. *J. Alloy. Compd.* **709**, 172–178 (2017).
36. Hagmann, J. A. et al. Molecular beam epitaxy growth and structure of self-assembled Bi_2Se_3/Bi_2MnSe_4 multilayer heterostructures. *New J. Phys.* **19**, 085002 (2017).
37. Eremeev, S. V., Otrokov, M. M. & Chulkov, E. V. New universal type of interface in the magnetic insulator/topological insulator heterostructures. *Nano Lett.* **18**, 6521–6529 (2018).
38. Mong, R. S. K., Essin, A. M. & Moore, J. E. Antiferromagnetic topological insulators. *Phys. Rev. B* **81**, 245209 (2010). This paper describes the first model of an antiferromagnetic topological insulator.
39. Lee, D. S. et al. Crystal structure, properties and nanostructuring of a new layered chalcogenide semiconductor, Bi_2MnTe_4. *CrystEngComm* **15**, 5532–5538 (2013).
40. Aliev, Z. S. et al. Novel ternary layered manganese bismuth tellurides of the MnTe-Bi_2Te_3 system: synthesis and crystal structure. *J. Alloy. Compd.* **789**, 443–450 (2019).
41. Zeugner, A. et al. Chemical aspects of the candidate antiferromagnetic topological insulator $MnBi_2Te_4$. *Chem. Mater.* **31**, 2795–2806 (2019).
42. Fang, C., Gilbert, M. J. & Bernevig, B. A. Topological insulators with commensurate antiferromagnetism. *Phys. Rev. B* **88**, 085406 (2013).
43. Yan, J.-Q. et al. Crystal growth and magnetic structure of $MnBi_2Te_4$. *Phys. Rev. Mater.* **3**, 064202 (2019).
44. Lee, S. H. et al. Spin scattering and noncollinear spin structure-induced intrinsic anomalous Hall effect in antiferromagnetic topological insulator $MnBi_2Te_4$. *Phys. Rev. Res.* **1**, 012011 (2019).
45. Lai, Y., Ke, L., Yan, J., McDonald, R. D. & McQueeney, R. J. Defect-driven ferrimagnetism and hidden magnetization in $MnBi_2Te_4$. *Phys. Rev. B* **103**, 184429 (2021).
46. Ding, L. et al. Crystal and magnetic structures of magnetic topological insulators $MnBi_2Te_4$ and $MnBi_4Te_7$. *Phys. Rev. B* **101**, 020412 (2020).
47. Riberolles, S. X. M. et al. Evolution of magnetic interactions in Sb-substituted $MnBi_2Te_4$. *Phys. Rev. B* **104**, 064401 (2021).
48. Vidal, R. C. et al. Surface states and Rashba-type spin polarization in antiferromagnetic $MnBi_2Te_4$(0001). *Phys. Rev. B* **100**, 121104 (2019).
49. Hao, Y.-J. et al. Gapless surface Dirac cone in antiferromagnetic topological insulator $MnBi_2Te_4$. *Phys. Rev. X* **9**, 041038 (2019).
50. Li, H. et al. Dirac surface states in intrinsic magnetic topological insulators $EuSn_2As_2$ and $MnBi_{2n}Te_{3n+1}$. *Phys. Rev. X* **9**, 041039 (2019).
51. Chen, Y. J. et al. Topological electronic structure and its temperature evolution in antiferromagnetic topological insulator $MnBi_2Te_4$. *Phys. Rev. X* **9**, 041040 (2019).
52. Shikin, A. et al. Nature of the Dirac gap modulation and surface magnetic interaction in axion antiferromagnetic topological insulator $MnBi_2Te_4$. *Sci. Rep.* **10**, 13226 (2020).
53. Yan, C. et al. Origins of electronic bands in the antiferromagnetic topological insulator $MnBi_2Te_4$. *Phys. Rev. B* **104**, L041102 (2021).
54. Nevola, D. et al. Coexistence of surface ferromagnetism and a gapless topological state in $MnBi_2Te_4$. *Phys. Rev. Lett.* **125**, 117205 (2020).
55. Swatek, P. et al. Gapless Dirac surface states in the antiferromagnetic topological insulator $MnBi_2Te_4$. *Phys. Rev. B* **101**, 161109 (2020).
56. Nevola, D. et al. On the role of defects in the electronic structure of $MnBi_{2-x}Sb_xTe_4$. arXiv preprint arXiv:2206.14325 (2022).
57. Bielinski, N. et al. Floquet–Bloch manipulation of the Dirac gap in a topological antiferromagnet. *Nat. Phys.* **21**, 458–463 (2025).
58. Shikin, A. M. et al. Sample-dependent Dirac-point gap in $MnBi_2Te_4$ and its response to applied surface charge: a combined photoemission and ab initio study. *Phys. Rev. B* **104**, 115168 (2021).
59. Hou, F. et al. Te-vacancy-induced surface collapse and reconstruction in antiferromagnetic topological insulator $MnBi_2Te_4$. *ACS Nano* **14**, 11262–11272 (2020).
60. Yuan, Y. et al. Electronic states and magnetic response of $MnBi_2Te_4$ by scanning tunneling microscopy and spectroscopy. *Nano Lett.* **20**, 3271–3277 (2020).
61. Chen, W., Zhao, Y., Yao, Q., Zhang, J. & Liu, Q. Koopmans' theorem as the mechanism of nearly gapless surface states in self-doped magnetic topological insulators. *Phys. Rev. B* **103**, L201102 (2021).
62. Garrity, K. F., Chowdhury, S. & Tavazza, F. M. Topological surface states of $MnBi_2Te_4$ at finite temperatures and at domain walls. *Phys. Rev. Mater.* **5**, 024207 (2021).
63. Bian, Q. et al. Correlated topological electronic states and surface magnetic orderings in layered $MnBi_2Te_4$. *Mater. Today Electron.* **5**, 100050 (2023).
64. Sass, P. M., Kim, J., Vanderbilt, D., Yan, J. & Wu, W. Robust *a*-type order and spin-flop transition on the surface of the antiferromagnetic topological insulator $MnBi_2Te_4$. *Phys. Rev. Lett.* **125**, 037201 (2020).
65. Liang, Z. et al. Mapping Dirac fermions in the intrinsic antiferromagnetic topological insulators $(MnBi_2Te_4)(Bi_2Te_3)_n$ (n = 0,1). *Phys. Rev. B* **102**, 161115 (2020).
66. Garnica, M. et al. Native point defects and their implications for the Dirac point gap at $MnBi_2Te_4$(0001). *npj Quantum Mater.* **7**, 7 (2022).
67. Tan, H. & Yan, B. Distinct magnetic gaps between antiferromagnetic and ferromagnetic orders driven by surface defects in the topological magnet $MnBi_2Te_4$. *Phys. Rev. Lett.* **130**, 126702 (2023).
68. Liu, Y. et al. Site mixing for engineering magnetic topological insulators. *Phys. Rev. X* **11**, 021033 (2021).
69. Liu, M. et al. Visualizing the interplay of Dirac mass gap and magnetism at nanoscale in intrinsic magnetic topological insulators. *Proc. Natl. Acad. Sci. USA* **119**, e2207681119 (2022).
70. Li, Q. et al. Imaging the breakdown and restoration of topological protection in magnetic topological insulator $MnBi_2Te_4$. *Adv. Mater.* **36**, 2312004 (2024).
71. Huang, Z., Du, M.-H., Yan, J. & Wu, W. Native defects in antiferromagnetic topological insulator $MnBi_2Te_4$. *Phys. Rev. Mater.* **4**, 121202 (2020).
72. Sahoo, M. et al. Ubiquitous order-disorder transition in the Mn antisite sublattice of the $(MnBi_2Te_4)(Bi_2Te_3)_n$ magnetic topological insulators. *Adv. Sci.* **11**, 2402753 (2024).
73. Estyunin, D. A. et al. Signatures of temperature driven antiferromagnetic transition in the electronic structure of topological insulator $MnBi_2Te_4$. *APL Mater.* **8**, 021105 (2020).
74. Chen, Y. L. et al. Massive Dirac fermion on the surface of a magnetically doped topological insulator. *Science* **329**, 659–662 (2010).
75. Xu, S.-Y. et al. Hedgehog spin texture and Berry's phase tuning in a magnetic topological insulator. *Nat. Phys.* **8**, 616–622 (2012).
76. Alfonsov, A. et al. Strongly anisotropic spin dynamics in magnetic topological insulators. *Phys. Rev. B* **103**, L180403 (2021).
77. Alfonsov, A. et al. Magnetic-field tuning of the spin dynamics in the magnetic topological insulators $(MnBi_2Te_4)(Bi_2Te_3)_n$. *Phys. Rev. B* **104**, 195139 (2021).
78. Yan, J.-Q. et al. Evolution of structural, magnetic, and transport properties in $MnBi_{2-x}Sb_xTe_4$. *Phys. Rev. B* **100**, 104409 (2019).

79. Chowdhury, S., Garrity, K. F. & Tavazza, F. Prediction of Weyl semimetal and antiferromagnetic topological insulator phases in Bi_2MnSe_4. *npj Comput. Mater.* **5**, 33 (2019).
80. Wimmer, S. et al. Mn-rich $MnSb_2Te_4$: a topological insulator with magnetic gap closing at high Curie temperatures of 45-50 K. *Adv. Mater.* **33**, 2102935 (2021).
81. Lee, S. H. et al. Evidence for a magnetic-field-induced ideal type-II Weyl state in antiferromagnetic topological insulator $Mn(Bi_{1-x}Sb_x)_2Te_4$. *Phys. Rev. X* **11**, 031032 (2021).
82. Zhu, T. et al. Synthesis, magnetic properties, and electronic structure of magnetic topological insulator $MnBi_2Se_4$. *Nano Lett.* **21**, 5083–5090 (2021).
83. Cao, L. et al. Growth and characterization of the dynamical axion insulator candidate $Mn_2Bi_2Te_5$ with intrinsic antiferromagnetism. *Phys. Rev. B* **104**, 054421 (2021).
84. Eremeev, S. V., Otrokov, M. M., Ernst, A. & Chulkov, E. V. Magnetic ordering and topology in $Mn_2Bi_2Te_5$ and $Mn_2Sb_2Te_5$ van der Waals materials. *Phys. Rev. B* **105**, 195105 (2022).
85. Watanabe, R. et al. Enhancement of anomalous Hall effect in epitaxial thin films of intrinsic magnetic topological insulator $MnBi_2Te_4$ with Fermi-level tuning. *Appl. Phys. Lett*. **120**, 031901 (2022).
86. Lüpke, F. et al. Anti-site defect-induced disorder in compensated topological magnet $MnBi_{2-x}Sb_xTe_4$. *Commun. Mater.* **4**, 82 (2023).
87. Petrov, E. K. et al. Domain wall induced spin-polarized flat bands in antiferromagnetic topological insulators. *Phys. Rev. B* **103**, 235142 (2021).
88. Fukushima, R. et al. Direct evidence of induced magnetic moment in Se and the role of misplaced Mn in $MnBi_2Se_4$-based intrinsic magnetic topological insulator heterostructures. *Phys. Rev. Mater.* **8**, 084202 (2024).
89. Eremeev, S. V. et al. Topological magnetic materials of the $(MnSb_2Te_4)\cdot(Sb_2Te_3)_n$ van der Waals compounds family. *J. Phys. Chem. Lett.* **12**, 4268 (2021).
90. Chen, B. et al. Intrinsic magnetic topological insulator phases in the Sb doped $MnBi_2Te_4$ bulks and thin flakes. *Nat. Commun.* **10**, 4469 (2019).
91. Lei, C., Chen, S. & MacDonald, A. H. Magnetized topological insulator multilayers. *Proc. Natl. Acad. Sci. USA* **117**, 27224–27230 (2020).
92. Xi, M. et al. Relationship between antisite defects, magnetism, and band topology in $MnSb_2Te_4$ crystals with $T_C \approx 40$ K. *J. Phys. Chem. Lett*. **13**, 10897–10904 (2022).
93. Chong, S. K. et al. Anomalous Landau quantization in intrinsic magnetic topological insulators. *Nat. Commun.* **14**, 4805 (2023).
94. Zhu, J. et al. Magnetic and electrical transport study of the antiferromagnetic topological insulator Sn-doped $MnBi_2Te_4$. *Phys. Rev. B* **103**, 144407 (2021).
95. Qian, T. et al. Magnetic dilution effect and topological phase transitions in $(Mn_{1-x}Pb_x)Bi_2Te_4$. *Phys. Rev. B* **106**, 045121 (2022).
96. Estyunin, D. A. et al. Comparative study of magnetic properties of $(Mn_{1-x}A^{IV}_x)Bi_2Te_4$ A^{IV} = Ge, Pb, Sn. *Magnetochemistry* **9**, 210 (2023).
97. Frolov, A. S. et al. Magnetic Dirac semimetal state of $(Mn,Ge)Bi_2Te_4$. *Commun. Phys.* **7**, 180 (2024).
98. Souchay, D. et al. Layered manganese bismuth tellurides with $GeBi_4Te_7$-and $GeBi_6Te_{10}$-type structures: towards multifunctional materials. *J. Mater. Chem. C.* **7**, 9939–9953 (2019).
99. Jahangirli, Z. A. et al. Electronic structure and dielectric function of Mn-Bi-Te layered compounds. *J. Vac. Sci. Technol. B* **37**, 062910 (2019).
100. Amiraslanov, I. R. et al. Crystal structure and Raman-active lattice vibrations of magnetic topological insulators $MnBi_2Te_4\cdot n(Bi_2Te_3)$ ($n = 0, 1,..., 6$). *Phys. Rev. B* **106**, 184108 (2022).
101. Zverev, V. N. et al. Transport properties of the magnetic topological insulators family $(MnBi_2Te_4)(Bi_2Te_3)_m$ ($m = 0, 1,\ldots, 6$). *JETP Lett*. **118**, 905–910 (2023).
102. Vidal, R. C. et al. Topological electronic structure and intrinsic magnetization in $MnBi_4Te_7$: A Bi_2Te_3 derivative with a periodic Mn sublattice. *Phys. Rev. X* **9**, 041065 (2019).
103. Wu, J. et al. Natural van der Waals heterostructural single crystals with both magnetic and topological properties. *Sci. Adv*. **5**, eaax9989 (2019).
104. Hu, C. et al. A van der Waals antiferromagnetic topological insulator with weak interlayer magnetic coupling. *Nat. Commun.* **11**, 97 (2020).
105. Klimovskikh, I. I. et al. Tunable 3D/2D magnetism in the $(MnBi_2Te_4)(Bi_2Te_3)_m$ topological insulators family. *npj Quantum Mater.* **5**, 54 (2020).
106. Wu, X. et al. Distinct topological surface states on the two terminations of $MnBi_4Te_7$. *Phys. Rev. X* **10**, 031013 (2020).
107. Lu, R. et al. Half-magnetic topological insulator with magnetization-induced Dirac gap at a selected surface. *Phys. Rev. X* **11**, 011039 (2021).
108. Shao, J. et al. Pressure-tuned intralayer exchange in superlattice-like $MnBi_2Te_4/(Bi_2Te_3)_n$ topological insulators. *Nano Lett.* **21**, 5874–5880 (2021).
109. Zhang, R.-X., Wu, F. & Das Sarma, S. Möbius insulator and higher-order topology in $MnBi_{2n}Te_{3n+1}$. *Phys. Rev. Lett.* **124**, 136407 (2020).
110. Hu, C. et al. Realization of an intrinsic ferromagnetic topological state in $MnBi_8Te_{13}$. *Sci. Adv.* **6**, eaba4275 (2020).
111. Tanaka, Y., Takahashi, R., Zhang, T. & Murakami, S. Theory of inversion-$\mathbb{Z}_4$ protected topological chiral hinge states and its applications to layered antiferromagnets. *Phys. Rev. Res.* **2**, 043274 (2020).
112. Gu, M. et al. Spectral signatures of the surface anomalous Hall effect in magnetic axion insulators. *Nat. Commun.* **12**, 3524 (2021).
113. Zhan, F. et al. Design of antiferromagnetic second-order band topology with rotation topological invariants in two dimensions. *Nano Lett.* **24**, 7741–7747 (2024).
114. Roy, B. Higher-order topological superconductors in $\mathcal{P}$-, $\mathcal{T}$-odd quadrupolar Dirac materials. *Phys. Rev. B* **101**, 220506 (2020).
115. Tcakaev, A.-V. et al. Intermixing-driven surface and bulk ferromagnetism in the quantum anomalous hall candidate $MnBi_6Te_{10}$. *Adv. Sci.* **10**, 2203239 (2023).
116. Yan, C. et al. Delicate ferromagnetism in $MnBi_6Te_{10}$. *Nano Lett.* **22**, 9815–9822 (2022).
117. Murakami, T. et al. Realization of interlayer ferromagnetic interaction in $MnSb_2Te_4$ toward the magnetic Weyl semimetal state. *Phys. Rev. B* **100**, 195103 (2019).
118. Kochetkova, E. et al. Mn interstitials in layered $Mn_{1+x}Sb_{2-2/3x}Te_4$: structural modification and Curie temperature boost. *Chem. Mater.* **37**, 1446–1456 (2025).
119. Chen, B. et al. Coexistence of ferromagnetism and topology by charge carrier engineering in the intrinsic magnetic topological insulator $MnBi_4Te_7$. *Phys. Rev. B* **104**, 075134 (2021).
120. Xie, H. et al. Charge carrier mediation and ferromagnetism induced in $MnBi_6Te_{10}$ magnetic topological insulators by antimony doping. *J. Phys. D Appl. Phys.* **55**, 104002 (2021).
121. Trang, C. X. et al. Crossover from 2D ferromagnetic insulator to wide band gap quantum anomalous Hall insulator in ultrathin $MnBi_2Te_4$. *ACS Nano* **15**, 13444–13452 (2021).
122. Zhao, Y.-F. et al. Even–odd layer-dependent anomalous Hall effect in topological magnet $MnBi_2Te_4$ thin films. *Nano Lett.* **21**, 7691–7698 (2021).
123. Wang, J., Lian, B., Qi, X.-L. & Zhang, S.-C. Quantized topological magnetoelectric effect of the zero-plateau quantum anomalous Hall state. *Phys. Rev. B* **92**, 081107 (2015).
124. Liu, C. et al. Robust axion insulator and Chern insulator phases in a two-dimensional antiferromagnetic topological insulator. *Nat. Mater.* **19**, 522–527 (2020). This paper reports the observation of the axion insulator state in the $MnBi_2Te_4$ thin flakes for the first time.

125. Mogi, M. et al. Tailoring tricolor structure of magnetic topological insulator for robust axion insulator. *Sci. Adv.* **3**, eaao1669 (2017).
126. Xiao, D. et al. Realization of the axion insulator state in quantum anomalous Hall sandwich heterostructures. *Phys. Rev. Lett.* **120**, 056801 (2018).
127. Gao, A. et al. Layer Hall effect in a 2D topological axion antiferromagnet. *Nature* **595**, 521–525 (2021). This paper reports the first observation of the layer Hall effect.
128. Gao, A. et al. An antiferromagnetic diode effect in even-layered $MnBi_2Te_4$. *Nat. Electron.* **7**, 751–759 (2024). This paper reports the observation of antiferromagnetic diode effect in the $MnBi_2Te_4$ thin flakes.
129. Fijalkowski, K. M. et al. Any axion insulator must be a bulk three-dimensional topological insulator. *Phys. Rev. B* **103**, 235111 (2021).
130. Zhuo, D. et al. Axion insulator state in hundred-nanometer-thick magnetic topological insulator sandwich heterostructures. *Nat. Commun.* **14**, 7596 (2023).
131. Qiu, J.-X. et al. Axion optical induction of antiferromagnetic order. *Nat. Mater.* **22**, 583–590 (2023). This paper reports the first observation of optical axion electrodynamics.
132. Gao, A. et al. Quantum metric nonlinear Hall effect in a topological antiferromagnetic heterostructure. *Science* **381**, 181–186 (2023). This paper probes the quantum metric of the $MnBi_2Te_4$ thin flakes.
133. Wang, N. et al. Quantum metric-induced nonlinear transport in a topological antiferromagnet. *Nature* **621**, 487 (2023). This paper probes the quantum metric of the $MnBi_2Te_4$ thin flakes.
134. Chen, R. et al. Layer Hall effect induced by hidden Berry curvature in antiferromagnetic insulators. *Natl Sci. Rev.* **11**, nwac140 (2024).
135. Malashevich, A. & Souza, I. Band theory of spatial dispersion in magnetoelectrics. *Phys. Rev. B* **82**, 245118 (2010).
136. Ahn, J., Xu, S.-Y. & Vishwanath, A. Theory of optical axion electrodynamics and application to the Kerr effect in topological antiferromagnets. *Nat. Commun.* **13**, 7615 (2022). This paper introduces a theory of axion electrodynamics at general frequencies.
137. Li, H. et al. Quantum geometry quadrupole-induced third-order nonlinear transport in antiferromagnetic topological insulator $MnBi_2Te_4$. *Nat. Commun.* **15**, 7779 (2024).
138. Deng, Y. et al. Magnetic-field-induced quantized anomalous Hall effect in intrinsic magnetic topological insulator $MnBi_2Te_4$. arXiv preprint arXiv:1904.11468 (2019).
139. Liu, C. et al. Quantum phase transition from axion insulator to Chern insulator in $MnBi_2Te_4$. arXiv preprint arXiv:1905.00715 (2019).
140. Deng, Y. et al. Quantum anomalous Hall effect in intrinsic magnetic topological insulator $MnBi_2Te_4$. *Science* **367**, 895–900 (2020). This paper reports the observation of the quantum anomalous Hall effect in the $MnBi_2Te_4$ thin flakes for the first time.
141. Cai, J. et al. Electric control of a canted-antiferromagnetic Chern insulator. *Nat. Commun.* **13**, 1668–1675 (2022).
142. Klitzing, K. V., Dorda, G. & Pepper, M. New method for high-accuracy determination of the fine-structure constant based on quantized Hall resistance. *Phys. Rev. Lett.* **45**, 494–497 (1980).
143. Ge, J. et al. High-Chern-number and high-temperature quantum Hall effect without Landau levels. *Natl Sci. Rev.* **7**, nwaa089 (2020). This paper reports the observation of the high-Chern-number high-temperature quantum Hall effect under external field without Landau levels in the $MnBi_2Te_4$ thin flakes.
144. Ovchinnikov, D. et al. Intertwined topological and magnetic orders in atomically thin Chern insulator $MnBi_2Te_4$. *Nano Lett.* **21**, 2544–2550 (2021).
145. Hu, C. et al. Growth, characterization, and Chern insulator state in $MnBi_2Te_4$ via the chemical vapor transport method. *Phys. Rev. Mater.* **5**, 124206 (2021).
146. Liu, C. et al. Magnetic-field-induced robust zero Hall plateau state in $MnBi_2Te_4$ Chern insulator. *Nat. Commun.* **12**, 4647–4653 (2021).
147. Ying, Z. et al. Experimental evidence for dissipationless transport of the chiral edge state of the high-field Chern insulator in $MnBi_2Te_4$ nanodevices. *Phys. Rev. B* **105**, 085412 (2022).
148. Bai, Y. et al. Quantized anomalous Hall resistivity achieved in molecular beam epitaxy-grown $MnBi_2Te_4$ thin films. *Natl Sci. Rev.* **11**, nwad189 (2023).
149. Li, Y. et al. Fabrication-induced even-odd discrepancy of magnetotransport in few-layer $MnBi_2Te_4$. *Nat. Commun.* **15**, 3399 (2024).
150. Zhu, J. et al. Direct observation of chiral edge current at zero magnetic field in a magnetic topological insulator. *Nat. Commun.* **16**, 963 (2025).
151. Wang, Y. et al. Towards the quantized anomalous Hall effect in AlO_x-capped $MnBi_2Te_4$. *Nat. Commun.* **16**, 1727 (2025).
152. Lian, Z. et al. Antiferromagnetic quantum anomalous Hall effect under spin flips and flops. *Nature* https://doi.org/10.1038/s41586-025-08860-z (2025).
153. Chong, S. K. et al. Pressure tunable quantum anomalous Hall states in a topological antiferromagnet. arXiv preprint arXiv:2306.10325 (2023).
154. Li, Y. et al. Reentrant quantum anomalous Hall effect in molecular beam epitaxy-grown $MnBi_2Te_4$ thin films. arXiv preprint arXiv:2401.11450 (2024).
155. Chen, C.-Z., Qi, J., Xu, D.-H. & Xie, X. Evolution of Berry curvature and reentrant quantum anomalous Hall effect in an intrinsic magnetic topological insulator. *Sci. China. Phys. Mech. Astron.* **64**, 127211 (2021).
156. Deng, H. et al. High-temperature quantum anomalous Hall regime in a $MnBi_2Te_4/Bi_2Te_3$ superlattice. *Nat. Phys.* **17**, 36–42 (2020).
157. Roychowdhury, S. et al. Giant topological Hall effect in the noncollinear phase of two-dimensional antiferromagnetic topological insulator $MnBi_4Te_7$. *Chem. Mater.* **33**, 8343–8350 (2021).
158. Takashiro, T. et al. Soft-magnetic skyrmions induced by surface-state coupling in an intrinsic ferromagnetic topological insulator sandwich structure. *Nano Lett.* **22**, 881–887 (2022).
159. Wu, M. et al. Novel $\pi/2$-periodic planar Hall effect due to orbital magnetic moments in $MnBi_2Te_4$. *Nano Lett.* **22**, 73–80 (2021).
160. Sun, H. et al. Rational design principles of the quantum anomalous Hall effect in superlatticelike magnetic topological insulators. *Phys. Rev. Lett.* **123**, 096401 (2019).
161. Ding, Y.-R., Xu, D.-H., Chen, C.-Z. & Xie, X. C. Hinged quantum spin Hall effect in antiferromagnetic topological insulators. *Phys. Rev. B* **101**, 041404 (2020).
162. Shao, D.-F., Ding, J., Gurung, G., Zhang, S.-H. & Tsymbal, E. Y. Interfacial crystal Hall effect reversible by ferroelectric polarization. *Phys. Rev. Appl.* **15**, 024057 (2021).
163. Chen, Z. et al. Topology-engineered orbital Hall effect in two-dimensional ferromagnets. *Nano Lett.* **24**, 4826 (2024).
164. Dai, W.-B., Li, H., Xu, D.-H., Chen, C.-Z. & Xie, X. C. Quantum anomalous layer Hall effect in the topological magnet $MnBi_2Te_4$. *Phys. Rev. B* **106**, 245425 (2022).
165. Hirahara, T. et al. Fabrication of a novel magnetic topological heterostructure and temperature evolution of its massive Dirac cone. *Nat. Commun.* **11**, 4821 (2020).
166. Kagerer, P. et al. Two-dimensional ferromagnetic extension of a topological insulator. *Phys. Rev. Res.* **5**, L022019 (2023).
167. Fukasawa, T. et al. Absence of ferromagnetism in $MnBi_2Te_4/Bi_2Te_3$ down to 6 K. *Phys. Rev. B* **103**, 205405 (2021).
168. Li, Q. et al. Large magnetic gap in a designer ferromagnet–topological insulator–ferromagnet heterostructure. *Adv. Mater.* **34**, 2107520 (2022).
169. Klimovskikh, I. I. et al. Interfacing two-dimensional and magnetic topological insulators: Bi bilayer on $MnBi_2Te_4$-family materials. *Mater. Today Adv.* **23**, 100511 (2024).

170. Ceccardi, M. et al. Anomalous Nernst effect in the topological and magnetic material $MnBi_4Te_7$. *npj Quantum Mater.* **8**, 76 (2023).
171. Bosnar, M., Vyazovskaya, A. Y., Petrov, E. K., Chulkov, E. V. & Otrokov, M. M. High Chern number van der Waals magnetic topological multilayers $MnBi_2Te_4$/hBN. *npj 2D Mater. Appl.* **7**, 33 (2023).
172. Jiang, J., Liu, X., Li, R. & Mi, W. Topological spin textures in a two-dimensional $MnBi_2(Se,Te)_4$ Janus material. *Appl. Phys. Lett*. **119**, 072401 (2021).
173. Li, Y. et al. Interplay between quantum anomalous Hall effect and magnetic skyrmions. *Proc. Natl. Acad. Sci. USA* **119**, e2122952119 (2022).
174. Peng, Y. & Xu, Y. Proximity-induced Majorana hinge modes in antiferromagnetic topological insulators. *Phys. Rev. B* **99**, 195431 (2019).
175. Dong, P. et al. Proximity-effect-induced superconductivity in a van der Waals heterostructure consisting of a magnetic topological insulator and a conventional superconductor. *Phys. Rev. B* **109**, L140503 (2024).
176. Yuan, W. et al. Coexistence of superconductivity and antiferromagnetism in topological magnet $MnBi_2Te_4$ films. *Nano Lett.* **24**, 7962–7971 (2024).
177. Perez-Piskunow, P. M. & Roche, S. Hinge spin polarization in magnetic topological insulators revealed by resistance switch. *Phys. Rev. Lett.* **126**, 167701 (2021).
178. An, Y. et al. Nanodevices engineering and spin transport properties of $MnBi_2Te_4$ monolayer. *npj Comput. Mater.* **7**, 45 (2021).
179. Li, S., Gong, M., Cheng, S., Jiang, H. & Xie, X. Dissipationless layertronics in axion insulator $MnBi_2Te_4$. *Natl Sci. Rev.* **11**, nwad262 (2024).
180. Varnava, N., Wilson, J. H., Pixley, J. & Vanderbilt, D. Controllable quantum point junction on the surface of an antiferromagnetic topological insulator. *Nat. Commun.* **12**, 3998 (2021).
181. Pixley, J., Varnava, N., Vanderbilt, D. & Wilson, J. Controlling a quantum point junction on the surface of an antiferromagnetic topological insulator. US Patent App. 17/690,627 (2022).
182. Yan, J.-Q., Huang, Z., Wu, W. & May, A. F. Vapor transport growth of $MnBi_2Te_4$ and related compounds. *J. Alloy. Compd.* **906**, 164327 (2022).
183. Hu, C., Qian, T. & Ni, N. Recent progress in $MnBi_{2n}Te_{3n+1}$ intrinsic magnetic topological insulators: crystal growth, magnetism and chemical disorder. *Natl. Sci. Rev.* **11**, nwad282 (2024).
184. Wang, P. et al. Intrinsic magnetic topological insulators. *Innovation* **2**, 100098 (2021).
185. Jiang, Z., Liu, J., Liu, Z. & Shen, D. A review of angle-resolved photoemission spectroscopy study on topological magnetic material family of $MnBi_2Te_4$. *Electron. Struct.* **4**, 043002 (2023).
186. Li, S. et al. Progress on the antiferromagnetic topological insulator $MnBi_2Te_4$. *Natl. Sci. Rev.* **11**, nwac296 (2024).
187. Shikin, A. M., Estyunin, D. A., Glazkova, D. A., Fil'nov, S. O. & Klimovskikh, I. I. Electronic and Spin Structures of Intrinsic Antiferromagnetic Topological Insulators of the $MnBi_2Te_4(Bi_2Te_3)_m$ Family and Their Magnetic Properties (Brief Review). *JETP Letters* **115**, 213–225 (2022).
188. Wang, A. et al. Observation of topological Anderson Chern insulator phase in $MnBi_4Te_7$ monolayer. arXiv preprint arXiv:2501.04354 (2025).
189. Qiu, J. X. et al. Observation of the axion quasiparticle in 2D $MnBi_2Te_4$. *Nature* https://doi.org/10.1038/s41586-025-08862-x (2025).
190. Xu, B. et al. Infrared study of the multiband low-energy excitations of the topological antiferromagnet $MnBi_2Te_4$. *Phys. Rev. B* **103**, L121103 (2021).

Acknowledgements

We thank Dr. I.I. Klimovskikh for stimulating discussions. We acknowledge the support by MCIN/AEI/10.13039/501100011033/ (Grant PID2022-138210NB-I00) and "ERDF A way of making Europe", by the Grant CEX2023-001286-S funded by MICIU/AEI/10.13039/501100011033, as well as MCIN with funding from European Union NextGenerationEU (PRTR-C17.I1) promoted by the Government of Aragon. A.Yu.V. acknowledges support from the Ministry of Science and Higher Education of the Russian Federation (state task No FSWM-2025-0009). E.V.C. acknowledges Saint-Petersburg State University for a research project No 125022702939-2. M.B. acknowledges support of the Croatian Science Foundation under the project numbers HRZZ-IP-2022-10-6321 and HRZZ-MOBDOL-2023-12-6938.

Author contributions

M.M.O. and E.V.C. conceived the idea and supervised the project. A.Yu.V., M.B., and M.M.O. made the literature analysis. A.Yu.V. and M.B. prepared the illustrations. All authors contributed to the writing of the manuscript.

Competing interests

The authors declare no competing interests.

Additional information

Supplementary information The online version contains supplementary material available at https://doi.org/10.1038/s43246-025-00794-3.

Correspondence and requests for materials should be addressed to Evgueni V. Chulkov or Mikhail M. Otrokov.

Peer review information *Communications Materials* thanks Tyler A. Cochran and the other, anonymous, reviewer(s) for their contribution to the peer review of this work. Primary Handling Editors: Aldo Isidori. A peer review file is available.